

Simulation of Exon Deletion Mutations Induced by Low-LET Radiation at the *HPRT* Locus

Werner Friedland,¹ Wei Bo Li, Peter Jacob and Herwig G. Paretzke

GSF-National Research Center for Environment and Health, Institute of Radiation Protection, 85764 Neuherberg, Germany

Friedland, W., Li, W. B., Jacob, P. and Paretzke, H. G. Simulation of Exon Deletion Mutations Induced by Low-LET Radiation at the *HPRT* Locus. *Radiat. Res.* **155**, 703–715 (2001).

The induction of *HPRT* mutants with exon deletions after irradiation with photons was simulated using the biophysical radiation track structure model PARTRAC. The exon-intron structure of the human *HPRT* gene was incorporated into the chromatin fiber model in PARTRAC. After γ and X irradiation, simulated double-stranded DNA fragments that overlapped with exons were assumed to result in exon deletion mutations with a probability that depended on the genomic or the geometric distance between the breakpoints. The consequences of different assumptions about this probability of deletion formation were evaluated on the basis of the resulting fractions of total, terminal and intragenic deletions. Agreement with corresponding measurements was obtained assuming a constant probability of deletion formation for fragments smaller than about 0.1 Mbp, and a probability of deletion formation decreasing with increasing geometric or genomic distance between the end points for larger fragments. For these two assumptions, yields of mutants with exon deletions, size distributions of deletions, patterns of deleted exons, and patterns of deleted STS marker sites surrounding the gene were calculated and compared with experimental data. The yields, size distributions and exon deletion patterns were grossly consistent, whereas larger deviations were found for the STS marker deletion patterns in this comparison. © 2001

by Radiation Research Society

INTRODUCTION

The hypoxanthine guanine phosphoribosyltransferase (*HPRT*) locus has been used in many investigations of the mutagenic action of ionizing radiation. The *HPRT* gene is located on the X-chromosome, is hemizygous, is nonessential, and has 9 exons distributed over about 40 kbp; *HPRT* mutants can be easily selected using the toxic drug 6-thioguanine (*I*).

¹ Author to whom correspondence should be addressed at GSF-National Research Center for Environment and Health, Institute of Radiation Protection, 85764 Neuherberg, Germany.

During the last several years, the multiplex polymerase chain reaction (PCR) technique has become a very useful tool for the molecular analysis of mutants by visualizing the presence or absence of individual exons of the *HPRT* gene (2–5). On the basis of their multiplex PCR patterns, the mutants are classified into three categories: (1) total deletions, if the PCR signals from all exons are lost; (2) partial deletions, where some exons are present in the PCR pattern while other exons are lost; and (3) mutants with a “normal” pattern consisting of point mutations including transitions, transversions, tandem base substitutions, frame-shifts and small deletions that are not detected by PCR.

Partial deletions are further subdivided into intragenic deletions and terminal deletions. In the first category, neither the first exon, 1, nor the last exon, 9, is deleted, and thus both breakpoints of the deletion are inside the gene. In the second category, either exon 1 or exon 9 is deleted. In addition to investigations of the exon deletion patterns, the end points of large deletions at the *HPRT* locus have been mapped using sequence tagged site (STS) primers and PCR amplification to probe for the presence of specific regions surrounding the gene (4, 6).

In the present paper, the induction of *HPRT* mutations with exon deletions after photon irradiation is used as an exercise to investigate, by comparison to experimental data, the capabilities of the biophysical track structure code PARTRAC and the detailed cellular DNA model developed previously to calculate such biological effects based on knowledge of the physical, chemical and biological mechanisms with a minimum of global model assumptions.

MATERIALS AND METHODS

Previous Simulations of Radiation-Induced HPRT Mutations

Biophysical simulations of radiation-induced *HPRT* mutations with exon deletions have been made by Hutchinson (7) and by Wu *et al.* (8). In both investigations, the following assumptions were used:

1. DNA lesions are distributed randomly along the DNA.
2. Deletions are the result of misrejoining of broken ends of DNA lesions.
3. The probability for misrejoining depends on the geometric distance between the breakpoints, which is closely related to the genomic distance.
4. Deletions are observed whenever any part of the deletion overlaps with an exon but not with an essential DNA sequence flanking the gene, because only surviving cells can be identified experimentally as mutants.

In these publications, the assumptions of the model regarding the initiating lesions, the misrejoining probability, and the relationship between genomic and geometric distance are diverse. Hutchinson (7) assumed that the probability for misrejoining is proportional to the collision rate of the two breakpoints that must meet to form a mutant with an exon deletion. Two cases were considered: If the initiating lesion results in a complete break on the chromatin, this rate is assumed to be proportional to $(1/r) \exp(-r/a)$ for breakpoints initially a distance r apart with a being the mean distance the diffusing structure must move before it is no longer available to form the deletion. If the lesion does not break the chromatin, the collision rate is assumed to be proportional to $\langle r^2 \rangle^{-3/2}$. For a chromatin fiber acting like a random coil polymer, the mean-square geometric distance (r^2) between the lesions is assumed to be proportional to the genomic distance m (9). The calculated size distributions of exon deletions of *HPRT* mutants were compared with experimental data for human and hamster cells. Good agreement was obtained when it was assumed that the chromatin was not broken. The assumption that the initiating lesion broke the chromatin led to discrepancies in the fractions of small, medium and large deletions. The author concluded that *HPRT* mutants with exon deletions could be caused by double-strand breaks in which the chromatin fiber is not broken, by other DNA lesions like single-strand nicks, or by the formation of a deletion by a single lesion interacting with undamaged DNA. Essential genes were assumed to be located 1.36 Mbp (3') and 5.75 Mbp (5') from the *HPRT* gene. However, the calculated results were not sensitive to the exact value used for the 5' distance.

In the other previous modeling on this topic, Wu *et al.* (8) assumed that a total-deletion mutation is produced by misrejoining of two DNA double-strand breaks (DSBs) from two separate tracks that are within a certain interaction distance at the time of their induction. The size distribution of total deletions was determined from a biphasic random-walk description of the interphase chromatin organization (10). A factor of 1/8 was used for the fraction of DSBs that will produce deletions; this fraction was derived by from misrejoining studies (11). An induction yield of 5.8 DSBs per Gbp and per Gy was used (11). Both the absolute frequency of *HPRT* mutants with total exon deletions and the length distribution were in agreement with experimental data for an assumed interaction distance of 0.75 μm . In the 3' direction, the flanking essential gene was assumed to be at a distance of 1.36 Mbp; in the 5' direction, the model predicted another essential gene at a distance of about 2.3 Mbp.

Both of the theoretical studies on exon deletions were focused primarily on larger deletions and were limited in their consideration of small deletions. In the paper of Hutchinson (7), the comparison with observed data on deletions in the human *HPRT* gene was made based on a classification of the deletions into the three groups: small, medium and large deletions. However, the class of small deletions consisted of all intragenic deletions and the terminal deletions in which adjacent markers at a distance of 0.4 and 0.76 Mbp were present; no comparisons between experiment and simulation were presented for subgroups of this class. Wu *et al.* restricted their study to total-deletion mutations; using the same formalism and parameters, the calculated frequencies of terminal and intragenic deletions would be significantly lower than the observed frequencies (8). The authors argued that accounting for the nucleosome periodicity or solenoid periodicity might explain the excess of small deletions. Indeed, an excess number of small DNA fragments has been determined experimentally after X, α -particle and heavy-ion irradiation (12–16), and theoretical investigations using higher-order DNA structures (15, 17–19) can explain these measurements.

Assumptions of the Present Calculations

1. Overview

In the present simulation, the following assumptions and methods were used:

- a. The induction and distribution of DSBs along the DNA is modeled on the basis of electron track structures from photon fields, accounting for the interaction physics and chemistry in charged-particle

tracks, overlaid with higher-order structures of the DNA. Details of the computer simulations of DNA structures, particle track structures, and DNA strand breakage are given below and elsewhere (18, 19).

- b. Deletions result from pairs of DSBs that are misrejoined. Pairs of breaks produced by single photons and pairs produced by two independent photons are included in the simulation.
- c. The probability of the formation of a deletion from a pair of DSBs is assumed to be a function of the geometric distance between the two breakpoints and/or the corresponding genomic distance.
- d. The relationship between geometric and genomic distance results from the structure of the chromosomes in the DNA model used in the present simulation.
- e. Exon deletions are observed whenever any part of the deletion overlaps with the coding region of an exon but not with any essential DNA sequences flanking the gene at a genomic distance of about 1.4 and 2.3 Mbp; more details about the simulation method are given below.
- f. For several assumptions and parameter values for the probability of deletion formation function, the relationship between exon deletion types (total, terminal, intragenic), the relationship between exon deletion sizes (small, medium, large), and the yields of mutants with exon deletions are determined.
- g. Functions and parameter values for the probability of deletion formation are selected which produce an overall agreement between the simulated and experimental relationships for deletion types and deletion sizes.
- h. Further simulation results obtained with these selected probability of deletion formation functions, including size distributions of deletions, exon deletion patterns, and STS marker deletion patterns, are presented and are compared with corresponding experimental results.

2. DNA target model

The DNA target model describes in a computer database the genome of a human cell nucleus on an atomic basis with six levels of DNA organization: deoxynucleotide pair, double helix, nucleosome, chromatin fiber, chromatin fiber loops, and chromosome domains. The chromatin fiber structure in this database is defined by a set of parameters, particularly fiber radius, length of linker DNA, angle between two neighboring nucleosomes, and number of nucleosomes per fiber length. In our model, these parameters describe regular solenoidal, crossed-linker and zigzag structures as well as stochastic arrangements of nucleosomes in the chromatin fiber. To specify a loop in the chromatin fiber, two basic fiber elements curved 11.25° to the right and to the left are introduced along with a third straight fiber element (see Fig. 1). All these elements can be stacked together. This approach provides a smooth interconnection of the lower-order DNA structures. The total DNA in a human cell nucleus is represented in the present simulation by a large number of identical fiber loops (64,230 loops each of 91 kbp genomic length) which is still manageable in a computer database for calculations of radiation interaction.

For the computer simulation of chromosomes, these chromatin fiber loops were assumed to be closely interconnected. Each new chromatin fiber loop starts near the final element of the former fiber loop, with a small deflection angle. During the construction of each fiber loop, the simulation can control whether its loop elements overlap with elements of loops established previously. In this case, the orientation and, if that is not sufficient, the starting point of the first loop element are varied until no overlap occurs. A territorial organization of the 46 human chromosomes is simulated by separating the spherical volume of the cell nucleus into domains with volumes corresponding to the chromosomal sizes. The domains are established on a regular grid of $101 \times 101 \times 101$ cubes, with sides 65 nm long, surrounding the cell nucleus. The total number of chromatin fiber loops in the simulation is assigned to the 46 chromosomes. During the construction of each chromosome, the connected fiber loops are limited to the volume of the cubes that were as-

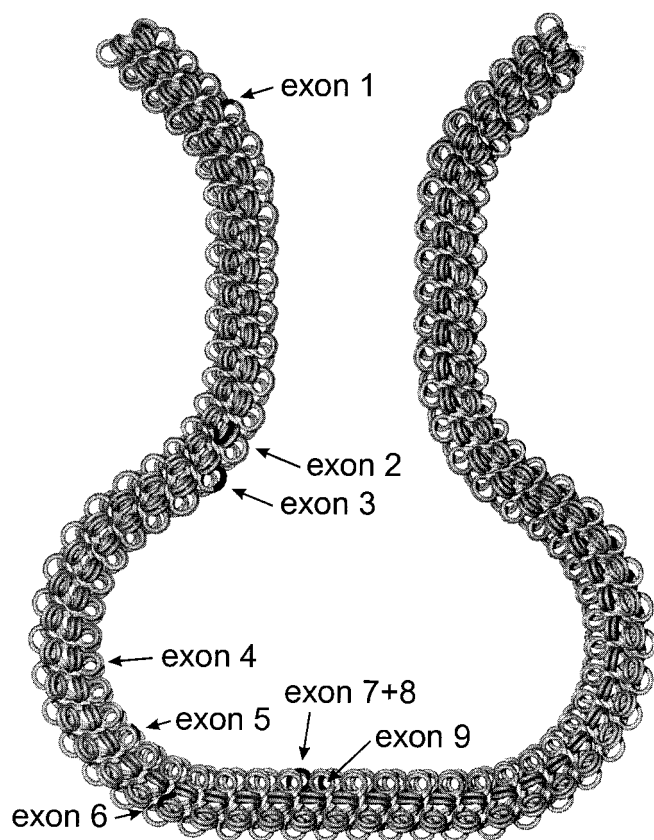


FIG. 1. Position of exons of the human *HPRT* gene projected onto a chromatin fiber loop with a crossed-linker structure.

signed to that chromosome. The hydration water shell around the DNA double helix is modeled according to Michalik and Begusova (20). Energy deposition events are scored as occurring in the water shell when they are located within the union of all spherical volumes of 0.35 nm radius centered at each DNA atom, but fall outside the van der Waals radii of the atoms themselves. Further details of the DNA target model are given elsewhere (18, 19). The DNA target model used in the present simulation is identical to that used by Friedland *et al.* (19); its main parameters are given in Table 1.

3. Computer simulation of particle track structures

The detailed histories of all secondary electrons of the incident photon field are followed in an event-by-event Monte Carlo simulation, in a geometry consisting of regions of homogeneous materials. The interactions of photons by the photoelectric effect (including Auger electrons and fluorescence electron emission), by the Compton effect, and by coherent scattering are simulated on the basis of a mixture of the respective elemental cross sections. The interactions of secondary electrons with the target material are calculated using the inelastic scattering cross sections for the model substance liquid water derived by Dingfelder *et al.* (21). Because water is the major component of cells, and because the electron energy loss in solid, dry DNA is very similar to that in liquid water (22), this simulation of the track structure would be expected to be a reasonable approximation of the energy deposition pattern inside the cell nucleus. Ionizations and excitations (= events) that occur inside a sphere corresponding to the cell nucleus are analyzed further.

From the superposition of the DNA target model with the simulated track structures, events falling inside one van der Waals radius of the DNA atoms are scored as "direct hits". Events occurring inside the water shell are classified into three categories: (a) For the volume attached to phosphate group atoms, 60% of the events are considered to "quasi-

TABLE 1
Parameters of the DNA Model Used in the Simulation

Cell diameter	20 μm
Cell height	16 μm
Cell nucleus diameter	13 μm
Chromatin fiber diameter	30 nm
Chromatin fiber structure	regular crossed linker
Nucleosomes per fiber element	7
Height of fiber element	13 nm
Base pairs per fiber element	1358
Fiber elements per loop	67
Loops per cell nucleus	64,230
Distance between succeeding loops	30 ± 10 nm
Angular deflection between loops	$\pm 60^\circ$
Minimum distance between fiber elements	30 nm

direct" hits and are processed further like direct hits, and 40% are processed further along the indirect, chemical pathway, which is described below. (b) For the volume attached to sugar group atoms, all events are followed in their chemical pathways. (c) For the volume attached to bases, all events are presumed to result in base damage, which is not considered further here. The water shell is assumed to be attached to the atoms nearest to the surface of its van der Waals sphere. It is further assumed that events occurring inside histones (simulated by spheres with a radius of 3.3 nm) cannot lead to DNA strand breaks through either direct or indirect pathways. All other excitations and ionizations in the vicinity of the chromatin fiber are assumed to occur in the bulk water and to undergo radiation chemistry.

Electrons with energies too low to excite electronic states of a water molecule are assumed to thermalize and to become solvated during the physico-chemical stage. Ionized and excited water molecules are assumed to dissociate or to relax, following a scheme adapted to obtain the reported initial yields of water radiolysis products (23). The subsequent diffusion and reaction of chemical species from 10^{-12} s to 10^{-6} s after irradiation is simulated using a step-by-step approach, following the general scheme proposed by Turner *et al.* (24). Reaction radii derived from Buxton *et al.* (25) are used to model the interaction of OH^\cdot with constituents of the DNA. In addition, the OH^\cdot are assumed to be scavenged by histones and molecules not explicitly considered in the simulation, with a scavenging capacity of $4 \times 10^8 \text{ s}^{-1}$. The dissociation schemes of excited states, reaction rate constants, and diffusion coefficients used in the simulation are given by Friedland *et al.* (19); further details of the radiation chemistry simulations are given by Ballarini *et al.* (26).

4. Simulation of DNA strand breakage and fragmentation

In PARTRAC, the direct and quasi-direct hits occurring at atoms in the DNA, as well as interactions of OH^\cdot with such atoms, are analyzed in terms of DNA strand breaks and fragments. A DNA single-strand break (SSB) is assumed to occur in the DNA (a) if an ionization or an excitation involving a local energy deposition greater than the ionization threshold of 10.8 eV for liquid water (21) has been found inside an atom (i.e. within one van der Waals radius) of the sugar-phosphate backbone, (b) if this ionization/excitation event has been scored as a quasi-direct hit in the water shell attached to phosphate, or (c) if an OH^\cdot has interacted with the sugar moiety. These assumptions lead to calculated yields of SSBs consistent with experimental data (19). Single-strand breaks at adjacent nucleotides on the same strand are scored as a single break. Two SSBs on opposite strands within a genomic distance of no more than 10 bp are scored as one DSB. The production of DSBs from SSBs produced by different particle tracks is negligible and is not considered.

5. Simulation of exon deletions

To simulate the induction of exon deletions, those fragments which overlap with exons of the *HPRT* gene but do not extend beyond essential genes flanking the *HPRT* locus are extracted as "potential" deletions that may form exon deletions with a certain probability which is determined in a second step of the simulation. To allow this simulation, the sequence of exons and introns of the human *HPRT* gene has been superimposed onto our DNA model. Figure 1 shows our model of the exons of the *HPRT* gene in a fiber loop of the DNA. To improve the statistics and to obtain an arbitrary overlay of the exon structure with the nucleosomes in the chromatin fiber structure, this superposition is done 100 times with different offsets (gene starting points) chosen randomly over the interval from zero up to the difference between the fiber loop length and the gene length. The actual *HPRT* locus on chromosome X is not taken into account; instead, for reasons of efficiency, it is assumed that each fiber loop in the genome model after the other includes the *HPRT* locus. Vital genes are assumed to be located at the 16th loop in the 3' direction and at the 26th loop in the 5' direction; depending on the offset used in the actual analysis, this corresponds to a distance of 1.36–1.41 Mbp toward the telomere and 2.27–2.31 Mbp toward the centromere. If two DSBs are found on the loop carrying the *HPRT* locus, the intersection of the corresponding fragment with exons of the *HPRT* gene is determined for all offsets, and the resulting potential intragenic, terminal or total deletions are scored.

If more than two DSBs are encountered on one loop, either (a) only the fragment between the most distant breaks is considered or (b) each resulting DNA fragment is considered separately, using the same algorithm. For the selection of the probability of deletion formation functions and parameters, case (a) is adopted since the deletion pattern for case (b) is influenced by the overall misrejoining probability p_0 . The collection of simulation results is also presented for case (a). Adopting case (b), the production of noncontiguous deletions of exons has been shown after four or five DSBs on a single chromatin fiber loop. Such patterns of exon deletions have been found experimentally in the *HPRT* gene of V79 Chinese hamster cells after α -particle irradiation but not after X irradiation (5).

For each loop carrying at least one DSB, the simulation also tested whether another DSB is found within 15 loops in the 3' direction or within 25 loops in the 5' direction of the genome and whether the corresponding fragments intersect, depending on the offset, with at least one exon of the gene, to produce a potential terminal deletion or, perhaps, a potential total deletion. For loops without DSBs, the model also ascertains whether DSBs are found within the distance to the nearest essential genes in both directions; if so, a potential total deletion is scored.

The second step in the simulation of exon deletions is to determine the probability of deletion formation, i.e. the probability with which a potential deletion results in an exon deletion due to misrejoining of the broken ends. In the absence of solid *a priori* knowledge, the probability of deletion formation is used here as a free model calibration parameter, which modifies the calculated relationships between the total, terminal and intragenic exon deletions and the yield of mutants to match the corresponding experimental data. To this end, the following assumptions (F1) to (F6) were tested as probability of deletion formation functions p depending on the genomic size m of the deletion and/or the geometric distance r between the breakpoints with a critical distance R , a critical genomic size M , and an overall misrejoining probability p_0 as parameters:

- F1: $p = 0$ for $r \geq R$;
 F2: $p = p_0 \times (m/M)^{-3/2}$ for $m \geq M$;
 F3: $p = p_0 \times (r/R)^{-3}$ for $r \geq R$;
 F4: $p = p_0 \times (r/R)^{-3}$ for $m \geq M$ and $r \geq R$;
 F5: $p = p_0 \times (m/M)^{-1/2} \times \exp[-(m/M)^{1/2}]$
 for $m \geq 0.322 M$;

- F6: $p = p_0 \times (r/R)^{-1} \times \exp(-r/R)$
 for $r \geq 0.567 R$;
 and
 $p = p_0$ otherwise in each case F1 to F6.

Assumption F1 has been used in the simulation of Wu *et al.* (8); however, their assumption of the probability of finding the two end points of the deletion within an interaction distance R according to a biphasic random-walk model of the genome is replaced here by the actual incidence of this condition in our DNA target model. According to the simulation of Hutchinson (7), assumptions F2, F3 and F4 correspond to the assumption that deletions are induced by lesions that do not break the chromatin, and the probability of deletion formation depends either on the genomic distance between the end points (F2) or on the geometric distance between the breaks (F3 and F4). In assumption F4, the distance dependence is applied only to fragments larger than a critical value M . Correspondingly, assumptions F5 and F6 follow the simulation of Hutchinson for deletions formed by a break in the chromatin. Normalizing factors of $M^{1/2}$ and R have been introduced to obtain a dimensionless p_0 . For each of the six assumptions, the maximum probability of deletion formation is p_0 , since the assumed functional dependences are valid as long as this value is not exceeded. In the simulation, the probability of deletion formation is taken into account by the Monte Carlo method: Potential deletions are accepted as real exon deletions whenever a random number in the interval between 0 and 1 is less than the actual probability of deletion formation.

Simulation Calculations

Two data sets from a previous study (19) of DNA damage after irradiation with ^{60}Co γ rays and 220 kVp X rays have been analyzed as described above. The geometry of the simulation has been designed to model the irradiation of a human fibroblast having a cylindrical shape, with a spherical nucleus in its center, through a thin Mylar film (4 μm) with the photon beam oriented perpendicular to the film. The electron interaction probabilities were scaled from the model substance liquid water to a density of 1.06 g cm^{-3} inside the cell (plasma and nucleus) and to a density of 1.4 g cm^{-3} in the Mylar film. The main parameters of the simulated cell and the DNA target are listed in Table 1.

The relationship between the genomic distance and the geometric distance of two loci on a chromosome is an important determinant of the production of DNA fragments after exposure to ionizing radiation. In Fig. 2, the mean two-dimensionally projected geometric distance is plotted as a function of the genomic distance for the DNA model in the present work, for the random-walk giant loop model used by Wu *et al.* (8), and for the experimental data of Yokota *et al.* (27) obtained with nonswollen nuclei. The results of our model have been determined on the basis of distances between the centers of the fiber elements. The small deflection angle between succeeding fiber loops leads to a slight decrease in the average distance around 300 kbp. Nevertheless, our simulated data are in good agreement with the experimental results. The mean geometric distances used by Wu *et al.* are larger by a factor of about 2 in this genomic size range.

RESULTS

Yields of Potential Deletions

Our simulation of exon deletion mutations is based on the production of potential deletions, i.e. DNA fragments that overlap with exons of the *HPRT* gene but do not extend beyond the flanking essential genes. Figure 3 shows the frequency distribution of the size of all potential deletions for irradiation with 2 Gy of ^{60}Co γ rays, together with the corresponding distribution for deletions resulting from a

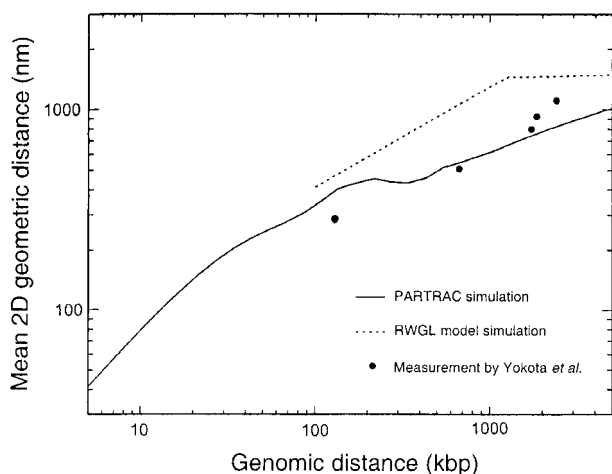


FIG. 2. Relationship between genomic and two-dimensionally projected geometric distance according to experiments with swollen nuclei under nonhypotonic conditions by Yokota *et al.* (29), the random-walk/giant loop model used by Wu *et al.* (8), and the chromatin in the present model.

single photon and the distribution calculated for a randomly broken stick. A relatively large deviation from the broken-stick distribution occurs in the first size interval; this reflects the increased production of these short DNA fragments due to pairs of breaks from single tracks. The distribution for potential deletions from independent tracks, i.e. the difference between the simulated distribution for all fragments and the simulated distribution for single-track fragments, agrees fairly well with the broken-stick distribution. The frequency of single-track fragments is almost independent of size for the interval between 0.2 and 2 Mbp.

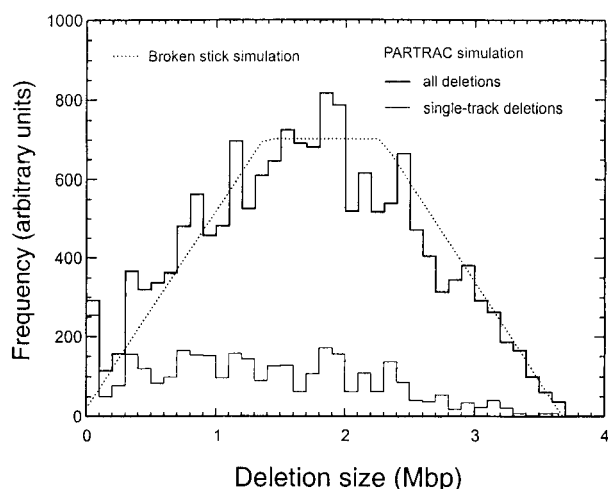


FIG. 3. Size distribution of “potential deletions” after irradiation with 2 Gy ^{60}Co γ rays according to the randomly broken stick model, the present simulation, and the contribution of single-track events to the present simulation.

The calculated yields of potential deletions, listed in Table 2, simulation P0, exceed the measured mutant frequencies by factors ranging from 20 to 70 for the data of Yamada *et al.* (4), ranging from 80 to 160 for the data of Park *et al.* (3), and of around 160 for the results of Nelson *et al.* (2).

Deletion Formation Probability Function

The formation of an actual deletion from a potential deletion is assumed to occur with a probability that is a function of the geometric distance, the genomic distance, or

TABLE 2
Yields of All Mutants with Exon Deletions and of Mutants with Total and with Partial Deletions from Experiments of Yamada *et al.* (4), Park *et al.* (3), and Nelson *et al.* (2) Compared with Simulated Results for Potential Deletions (P0) and for Deletion Formation Probability Functions P1 and P2 using the Values of p_0 in the Last Line to Adapt the Integrated Yield to the Measured Data

	Dose (Gy)	Yield of mutants per 10^6 cells										
		Experiment, ^{60}Co γ rays (4)	Simulation, ^{60}Co γ rays			Experiment, ^{60}Co γ rays (3)	Simulation, ^{60}Co γ rays		Experiment, 80 kV X rays (2)	Simulation, 220 kV X rays		
			P0	P1	P2		P1	P2		P0	P1	P2
All exon deletions	1	13	249	5.8	8.3	3	2.8	4.1		335	2.5	3.0
	2	18	873	16	19	12	8.0	9.3	6.8	1080	6.8	6.8
	3	29	1891	31	32	17	15	15		2266	13	11
	4	45	3206	51	46	19	25	23		3810	21	16
Total deletions	1	4	233	2.8	4.6	2	1.4	2.2		315	1.2	1.8
	2	5	825	9.4	10	4	4.6	5.1	3.6	1022	3.8	4.0
	3	17	1793	19	17	9	9.5	8.3		2150	8.1	6.7
	4	39	3044	33	25	16	16	12		3619	14	9.6
Partial deletions	1	9	16	2.9	3.8	1	1.4	1.8		20	1.3	1.2
	2	13	48	6.9	8.5	8	3.4	4.2	3.2	58	3.0	2.8
	3	12	98	12	15	8	5.8	7.2		116	5.2	4.7
	4	6	163	18	21	3	8.9	10		192	7.7	6.9
p_0			0.60	0.77		0.29	0.34			0.21	0.21	

Note. Fractions of partial and total deletions measured by Yamada *et al.* for the “low-dose” class (1–2 Gy) are applied to both dose values.

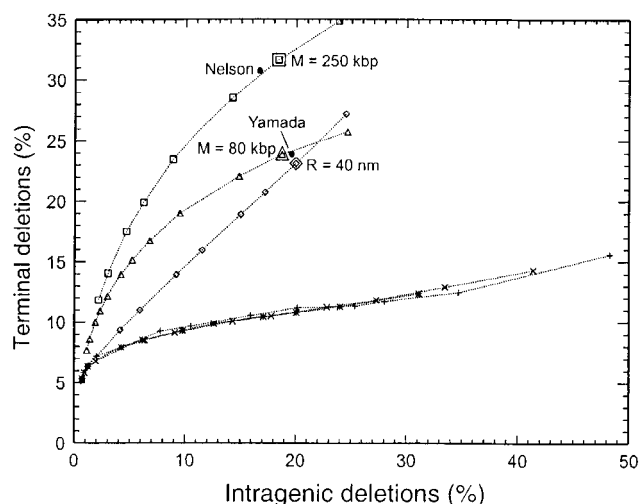


FIG. 4. Simulated percentages of terminal deletions and intragenic deletions after irradiation with 2 Gy ^{60}Co γ rays compared to the experimental data of Nelson *et al.* (2) and Yamada *et al.* (4). The percentage of total deletions is 100% minus the sum of the abscissa and ordinate values. The dotted lines are drawn to guide the eyes and connect the simulation results for different values of the parameters R (in nm: 1000, 500, 200, 150, 100, 80, 60, 50, 40, 30) and M (in kbp: 1000, 800, 600, 500, 400, 300, 250, 200, 150, 100, 80, 60) within the same probability of deletion formation function. (+) $p = 0$ for $r > R$; (*) $p = (r/R)^{-3}$ for $r > R$; (Δ) $p = (m/M)^{-3/2}$ for $m > M$; (\times) $p = (r/R)^{-1} \exp(-r/R)$ for $r > 0.567 R$; (\square) $p = (m/M)^{-1/2} \exp[-(m/M)^{-1/2}]$ for $m > 0.322 M$; (\diamond) $p = (r/R)^{-3}$ for $m > 150$ kbp and $r > R$; $p = 1$ otherwise in each case.

even both distances between the end points. In all these approaches, the factor p_0 is the maximum probability; it determines the absolute yield of mutants in the simulations but has almost no influence on the spectrum of deletion types, the size distributions, or the patterns of deleted exons or STS markers.

In Fig. 4, the calculated fractions of terminal deletions are plotted in relation to the fraction of intragenic deletions for the functional dependencies F1 to F6 of the probability of deletion formation after irradiation with a dose of 2 Gy ^{60}Co γ rays. The percentage of total deletions corresponds to 100% minus the sum of the x and y values in the figure. Additionally, the experimental distribution of deletion types measured by Yamada *et al.* (4) (pooled data for 1 to 4 Gy) and the distribution determined by Nelson *et al.* (2) after exposure to 2 Gy are included in the figure. The symbols represent simulations with individual choices of the parameter R , ranging from 30 nm to 1000 nm, or the parameter M , ranging from 60 kbp to 1 Mbp.

The three simulations with a probability of deletion formation that depends only on the geometric distance of the end points (F1, F3 and F6) result in almost the same selection of deletion type distribution patterns, which are characterized by a small fraction of terminal deletions of about 10%. On the other hand, the two genomic distance-dependent probability of deletion formation functions, F2 and F5, lead to comparable increases in the fractions of both terminal and intragenic deletions with decreasing critical dis-

tance M ; both can be brought into overall agreement with the experimentally determined relationship. Such an agreement can also be obtained for the probability function F4, where the dependence on the geometric distance is valid only for fragments greater than a certain length. In Fig. 4, results using F4 are plotted for a critical length of 150 kbp. With increasing critical length, the curve becomes steeper. The distributions of fragment types marked in the figure by larger symbols are close to the experimental results; they were obtained with the probability of deletion formation functions

$$\text{P1: } p = p_0 \times (m/80 \text{ kbp})^{-3/2} \quad \text{for } m \geq 80 \text{ kbp};$$

$$\text{P2: } p = p_0 \times (r/40 \text{ nm})^{-3} \quad \text{for } m \geq 150 \text{ kbp} \\ \text{and } r \geq 40 \text{ nm};$$

$$\text{P3: } p = p_0 \times (m/250 \text{ kbp})^{-1/2} \\ \times \exp[-(m/250 \text{ kbp})^{1/2}] \\ \text{for } m \geq 80 \text{ kbp};$$

with

$$p = p_0 \quad \text{otherwise in all three cases.}$$

The values of p_0 determine the yields of mutants; they are analyzed in the following section.

Another critical comparison used by Hutchinson to assess different assumptions about deletion induction is the distribution of small, medium and large deletions based on the presence or absence of STS markers (7). We adopt his definition of these three classes: Small deletions include mutants with intragenic and terminal deletions not extending beyond the DXS79 or the DXS86 marker at a distance of 0.4 and 0.8 Mbp from the *HPRT* gene; large deletions include mutants with deletions of all exons where at least one of these two markers is not found; medium deletions include the remaining fraction of mutants with total deletions. In Fig. 5, the simulated fractions of medium deletions are plotted as in relation to the fractions of small deletions after irradiation with 2 Gy of ^{60}Co γ rays for various parameter choices for the six probability of deletion formation functions, together with the experimental results of Yamada *et al.* (4) and Nelson *et al.* (6). As before, the three approaches with geometric distance-dependent functions produce similar curves, in which the fractions of medium deletions are smaller than the experimental results by factors of about 2. Again, the fractions for functions P1 and P2 with their specific parameter choices are in reasonable agreement with the measured data. For P3, however, the exponential dependence on the genomic distance between the end points results in a very small fraction of large deletions, which totally disagrees with the experimental results. Therefore, no further simulation results are presented for simulation P3.

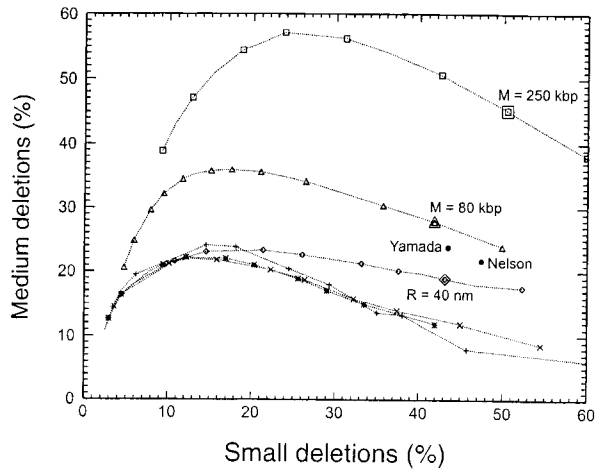


FIG. 5. Simulated percentages of medium deletions in relation to small deletions after irradiation with 2 Gy ^{60}Co γ rays compared to the experimental data of Nelson *et al.* (6) and Yamada *et al.* (4). The percentage of large deletions is 100% minus the sum of the abscissa and ordinate values. The dotted lines are drawn to guide the eyes and connect the simulation results for different values of the parameters R (in nm: 1000, 500, 200, 150, 100, 80, 60, 50, 40, 30) and M (in kbp: 1000, 800, 600, 500, 400, 300, 250, 200, 150, 100, 80, 60) within the same probability of deletion formation function. (+) $p = 0$ for $r > R$; (*) $p = (r/R)^{-3}$ for $r > R$; (Δ) $p = (m/M)^{-3/2}$ for $m > M$; (\times) $p = (r/R)^{-1} \exp(-r/R)$ for $r > 0.567 R$; (\square) $p = (m/M)^{-1/2} \exp[-(-m/M)^{-1/2}]$ for $m > 0.322 M$; (\diamond) $p = (r/R)^{-3}$ for $m > 150$ kbp and $r > R$; $p = 1$ otherwise in each case.

Dose-Dependent Yields of Mutants

In Table 2, measured and calculated dose-dependent yields of *HPRT* mutants with exon deletions are compared; calculated results for potential deletions are also included. The dose-integrated yield measured by Yamada *et al.* (4) agrees with the simulated result for the values $p_0 = 0.60$ and $p_0 = 0.77$ in functions P1 and P2, respectively. Corresponding values related to the measurements of Park *et al.* (3) and Nelson *et al.* (2) are between 0.21 and 0.34. The almost constant and, for the highest dose even decreasing, numbers of observed mutants with partial deletions are not seen in the simulated results. The numbers of simulated intragenic deletions increase linearly with dose; the numbers of simulated terminal deletions exhibit a linear-quadratic rise, like the numbers of simulated total deletions.

Probability of Deletion Formation

In Fig. 6, the probabilities of deletion formation after irradiation with 2 Gy of ^{60}Co γ rays according to simulation P1 with $p_0 = 0.6$ and simulation P2 with $p_0 = 0.77$ are presented as a function of the genomic distance together with the corresponding data from the simulation of Wu *et al.* (8). The data from the present work reflect the simulated relationship between exon deletions and potential deletions including the stochastic outcome of the Monte Carlo method. The distribution for simulation P2 is affected considerably by the random variation in the frequency of extraordinarily short geometric distances between two pieces of

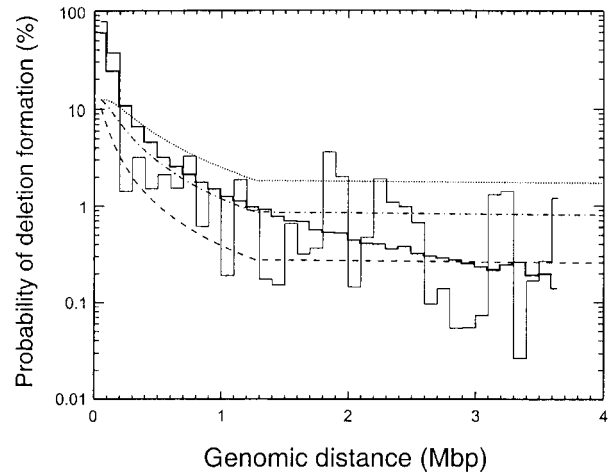


FIG. 6. Simulated probability of deletion formation after irradiation with 2 Gy ^{60}Co γ rays as a function of the genomic distance between the end points compared with a corresponding simulation of Wu *et al.* (8) for different interaction distances. The data of simulations P1 and P2 are fractions of potential deletions sampled by the Monte Carlo method. Simulation of Wu *et al.*: (---) 0.5 μm ; (- - -) 0.75 μm ; (- · - · -) 1 μm . Present work: (—●—) simulation P1; (—■—) simulation P2.

DNA with a genomic distance in the corresponding size interval.

Size Distribution of Mutants with Exon Deletions

In Fig. 7, the cumulative size distributions of mutants with exon deletions determined from the presence or absence of STS markers measured by Nelson *et al.* (6) and

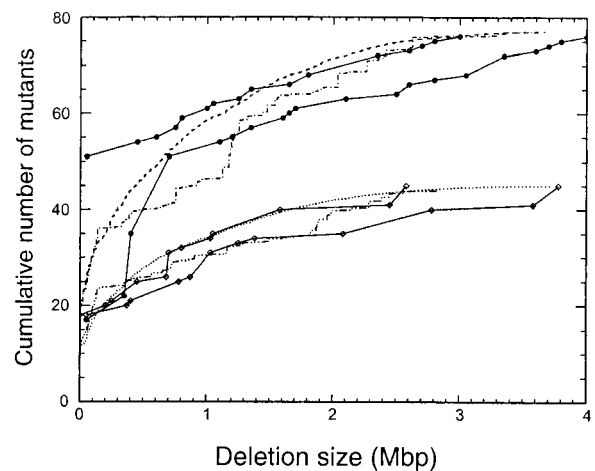


FIG. 7. Cumulative size distributions of mutants with exon deletions from simulations after irradiation with 2 Gy ^{60}Co γ rays and 220 kV X rays compared with experimental data of Nelson *et al.* (6) and Yamada *et al.* (4). The simulated results are normalized to the number of mutants in the experiments. The lower limits for the experimental data have been determined from the distances between terminal deleted STS markers or exons; the upper limits have been determined from the distances between flanking present STS markers or exons. (●—●) Experiment of Nelson *et al.* (6); (---) simulation P1, X rays; (- - -) simulation P2, X rays; (\diamond — \diamond) experiment of Yamada *et al.* (4); (·····) simulation P1, γ rays; (- · - · -) simulation P2, γ rays.

TABLE 3
Patterns of Deleted Exons According to Measurements from Yamada *et al.* (4) and from Nelson *et al.* (2) with Corresponding Expected Values from Simulations P1 and P2

Pattern of deleted exons									Number of mutants									
									Experiment			Simulation		Experiment			Simulation	
									⁶⁰ Co γ rays, 1–4 Gy (4)			⁶⁰ Co γ rays, 2 Gy		80 kV X rays, 2 Gy (2)			220 kV X rays, 2 Gy	
1	2	3	4	5	6	7-8	9		P1	P2		P1	P2					
X									2	3.0	3.0	8	4.6	4.2				
	X									1.2	1.4	1	2.1	1.9				
		X							1	1.4	1.5	2	2.2	2.2				
			X						3	1.3	1.6	2	2.5	2.4				
				X						1.2	1.2	4	2.1	2.0				
					X					1.2	1.4		2.3	2.3				
						X			3	1.3	1.4	3	2.4	2.3				
							X		3	1.2	1.3	2	2.1	2.2				
								X		0.21	0.23	1	0.4	0.3				
X	X								1	0.4	0.4		0.7	0.8				
	X	X							1	0.014	0.016		0.015	0.015				
		X	X						1	0.13	0.15	1	0.3	0.2				
			X	X						0.10	0.12		0.23	0.18				
						X	X			0.9	0.9	2	1.6	1.6				
X	X	X								1.2	1.2	4	2.0	1.3				
			X	X	X					0.08	0.08		0.12	0.11				
					X	X	X			0.4	0.4	1	0.6	0.7				
X	X	X	X						3	0.3	0.3		0.6	0.6				
				X	X	X	X			0.4	0.4	1	0.8	0.6				
X	X	X	X	X	X	X	X		3	0.3	0.26		0.6	0.5				
			X	X	X	X	X			1.1	1.0	3	2.1	2.0				
X	X	X	X	X	X	X	X			0.5	0.4		0.8	0.8				
		X	X	X	X	X	X			0.18	0.19	1	0.4	0.3				
X	X	X	X	X	X	X	X			0.16	0.15		0.3	0.3				
	X	X	X	X	X	X	X			1.3	1.3	1	2.5	2.1				
X	X	X	X	X	X	X	X		26	26.3	25.1	41	43.3	45.0				

Notes. The sum of expected mutants is scaled to the number of analyzed mutants in the experiments. Patterns not found in the experiments with a calculated number of mutants below 0.1 are not included in the table.

Yamada *et al.* (4) are compared with the corresponding simulated distributions scaled to the same total number of mutants. For the experimental distribution, only a lower and an upper limit can be given, due to the uncertainty in the position of the end points between absent and present STS markers. The experimental data and simulations are in overall accord.

Patterns of Deleted Exons

In Table 3, patterns of deleted exons in *HPRT* mutants from the experiments of Yamada *et al.* (4) and Nelson *et al.* (2) are compared with the corresponding simulated distributions of expected values normalized to the number of analyzed mutants with exon deletions. The pattern measured by Nelson *et al.* is in good agreement with the patterns of both simulations; the differences are not significant. The largest deviations are found for simulation P1 in the number of mutants with a deletion of only exon 1 and for simulation P2 in the pattern with deleted exons 1 to 3; based on Poisson statistics, such a random deviation occurs with a probability of 9.1% and 4.7% for P1 and P2, respectively. The experimental results of Yamada *et al.* are

reproduced to a smaller extent by the simulations; here some differences are significant. Particularly, the three observed mutants with terminal deletions of four exons as well as those with five deleted exons are inconsistent with corresponding expected numbers of about 0.3 in both simulations; the probability of random variation to such an extent is less than 0.5%.

Noncontiguous deletions are found in the simulations about once among 10,000 mutants with exon deletions. However, only one-tenth are visible as noncontiguous patterns of deleted exons, which corresponds to expected values of less than 0.001 for both experimental data sets (2, 4). The majority of noncontiguous deletions cannot be identified from the exon deletion pattern because the undeleted part of the gene between the deletions does not include a complete exon or because one of the deleted parts is located within an intron.

Patterns of Deleted STS Markers

In Table 4, the measured patterns of deleted STS markers flanking the *HPRT* locus determined by Yamada *et al.* (4) and by Nelson *et al.* (6) are compared with the correspond-

TABLE 4
Patterns of Deleted STS Markers in Mutants with Exon Deletions According to Measurements from Yamada *et al.* (4) and from Nelson *et al.* (6) with the Corresponding Expected Values from Simulations P1 and P2

Pattern of deleted markers										Number of mutants					
DXS53	299R	DXS79	931L/ yH3L	<i>HPRT</i> exon 1	<i>HPRT</i> exon 9	931R/ yH3R	DXS86	DXS10	DXS144	Experiment, ⁶⁰ Co γ rays, 1–4 Gy (4)	Simulation P1, ⁶⁰ Co γ rays, 2 Gy	Simulation P2, ⁶⁰ Co γ rays, 2 Gy	Experiment, 80 kV X rays, 2 Gy (2)	Simulation P1, 220 kV X rays, 2 Gy	Simulation P2, 220 kV X rays, 2 Gy
				X						8	2.6	3.0	13	4.4	3.4
			<	X							0.7	0.5		1.1	0.7
					X					3	2.5	3.1	9	4.2	4.2
					X	>					1.2	0.5		2.1	1.2
				X	X					1	9.4	6.6	16	14.1	8.6
				X	X	X				9	5.0	2.9	1	8.2	4.1
				X	X	X	X			2	0.8	0.6		1.4	2.2
				X	X	X	X	X			1.3	0.8	1	2.4	4.2
				X	X	X	X	X	X		0.0	0.0	1	0.0	0.0
			X	X	X						0.4	0.3		0.6	0.04
			X	X	X	X				3	0.4	0.3		0.7	0.9
			X	X	X	X	X				0.07	0.02		0.15	0.6
			X	X	X	X	X	X			0.15	0.07		0.24	0.3
		X	X	X	X						1.7	1.4	3	3.4	2.0
		X	X	X	X	X					1.8	1.1	4	3.0	4.5
		X	X	X	X	X	X				0.5	0.3	1	0.9	1.2
		X	X	X	X	X	X	X			0.7	1.5		1.5	1.3
	X	X	X	X	X					1	1.7	1.7	2	3.1	5.0
	X	X	X	X	X	X					2.5	3.9	2	4.6	6.1
	X	X	X	X	X	X	X			5	0.7	1.8		1.2	2.1
	X	X	X	X	X	X	X	X			1.3	2.7	1	2.4	4.3
X	X	X	X	X	X						0.4	1.2	1	0.9	1.5
X	X	X	X	X	X	X				1	0.7	1.3	4	1.2	2.8
X	X	X	X	X	X	X	X			4	0.20	0.24	2	0.4	0.3
X	X	X	X	X	X	X	X	X			0.4	1.0	2	0.9	1.5

Notes. The sum of expected values is scaled to the number of mutants analyzed in the experiments. The first four rows show results for terminal deletions, the other rows for total deletions. >: sum for one or more deleted markers in the 3' direction, <: sum for one or more deleted markers in the 5' direction. Patterns not found in the experiments with a calculated number of mutants below 0.1 are not included in the table.

ing expected values from the simulations. The two experimental data sets are rather discordant, particularly in the numbers of mutants with total exon deletions without marker deletions (16 out of 63 mutants compared to 1 out of 37 mutants) and with breakpoints between DXS79 and 299R (8/63 compared to 0/37). A common feature of the measured data is the lack of deleted STS markers among the 33 mutants with terminal deletions; according to the simulations, about 20% of the terminal deletions are expected to have deleted STS markers. The comparison between simulations and measurements of STS marker deletion patterns of mutants with total exon deletions shows reasonable agreement between the results of Nelson *et al.* (6) and simulation P1, except in the number of mutants in which only marker 931R is deleted. This discrepancy is smaller for simulation P2, but for many other patterns of deleted markers, the deviation from the experimental results is larger for P2 than for P1. The patterns measured by Yamada *et al.* (4) disagree with both simulations. The particular patterns of several deleted markers found in five and in four mutants, as well as the presence of only a single mutant with a total exon deletion but without deletion of flanking STS markers, are implausible on the basis of the simulated data.

DISCUSSION

Production of Potential Deletions

The first step in the present simulation model of radiation-induced exon deletion mutations in the human *HPRT* gene

is the production of potential deletions, i.e. double-stranded DNA fragments that overlap with exons but not with flanking essential genes. The production of DNA fragments is closely related to the induction of DNA DSBs. In the present simulation, the calculated DSB yield is 8.8 Gbp⁻¹ Gy⁻¹ for 220 kVp X rays and 8.1 Gbp⁻¹ Gy⁻¹ for ⁶⁰Co γ rays. These values are higher than results from typical experiments (28, 29) for the DSB yield after low-LET irradiation of cells, such as the value of 5.8 Gbp⁻¹ Gy⁻¹ used by Wu *et al.* (8). However, DSB yields determined from measurements of DNA fragment distributions after X irradiation were considerably larger [10.7 Gbp⁻¹ Gy⁻¹ (13) and 8.8 Gbp⁻¹ Gy⁻¹ (14)] than the values obtained by FAR analysis or other techniques (29). Recently, DSB induction after exposure to 80 kV X rays was determined at the *HPRT* region of different human and hamster cell lines, resulting in a yield of 9.8 Gbp⁻¹ Gy⁻¹ (30); this value has been proposed to be representative of the entire genome. Thus the results of our simulation of the induction of DSBs are in reasonable agreement with the available experimental data. The difference in X-ray energy between the simulation (220 kV) and the experiment of Nelson *et al.* (80 kV) is not expected to have a significant influence on DSB induction and DNA fragmentation.

The production of double-stranded DNA fragments includes fragments between two DSBs from independent tracks and between pairs of DSBs from a single track. The first fraction can be described by a randomly broken stick distribution. The second fraction depends on the character-

istics of the charged-particle track structure (e.g. LET, track length), which are not discussed further here, and on the geometric organization of the genome, especially the relationship between geometric and genomic distance. The geometric simulation of the genome affects the production of DNA fragments in many respects. The arrangement of nucleosomes in the chromatin fiber determines the size distributions of fragments in the range up to 2 kbp. The total yield of DNA fragments in this size interval, however, is determined primarily by the number of base pairs or nucleosomes per unit fiber length (18). For fragments up to about 30 kbp, the simulated fiber can be regarded as more or less straight; genomic and geometric distances are proportional to each other, and the production of fragments still depends mainly on the compactness of the DNA in the fiber. For larger fragment sizes, the relationship between genomic and geometric distances depends on the layout of the fiber loop and the interconnection of succeeding loops. The frequency of rather small geometric distances is probably a more important determinant than the average value for the generation of DNA fragments from single tracks. With increasing fragment size, the geometry-dependent contribution from single-track events decreases, e.g. from around 30% for 100-kbp fragments to about 10% for 1-Mbp fragments after irradiation with 1 Gy ^{60}Co γ rays (19). In conclusion, the simulation model of the genome is expected to give reasonable values for the distribution of pairs of DSBs, since the yields of DSBs, the yields of small DNA fragments (<2 kbp), and the relationship between genomic and geometric distance are in agreement with the available experimental data; however, between about 50 kbp and 1 Mbp, the uncertainties may be greater than those for smaller or larger DNA fragments.

Deletion Formation Probability Function

In our simulation, the assumptions of Wu *et al.* (8) of a 0.75- μm interaction distance and a probability of deletion formation of 0.125 within this distance led to calculated fractions of 6% terminal deletions and 1% intragenic exon deletions, which are in conflict with the experimental findings. In the simulations with a geometric distance-dependent probability of deletion formation, a rather small critical distance is necessary to reduce the fraction of total deletions to the measured value, but then the fraction of terminal deletions decreases far below the experimental result. The similarity of the curves in Fig. 4 for these three simulations indicates that the abruptness with which the probability of deletion formation decreases with increasing distance has little influence on the distribution of deletion types. Therefore, it can be expected that, for any purely geometric distance-dependent probability of deletion formation function, a simulation using the present DNA target model will not approach the measured distribution. This is probably a consequence of the projection of the gene onto a stiff chromatin fiber, which produces large geometric dis-

tances between distant exons. The result may be different for other representations of the genome, particularly if the geometric distances between the exons are reduced significantly.

The values of the parameters R and M in the probability of deletion formation functions for which the distributions of deletion types approach the experimental results of Yamada *et al.* (4) depend on the dose and on the photon energy used in the simulation. The data in Fig. 4 are calculated for a dose of 2 Gy of ^{60}Co γ rays, whereas the experimental results of Nelson *et al.* (2) were obtained after exposure to 2 Gy 80 kV X rays and the data of Yamada *et al.* were pooled for irradiations with 1–4 Gy of ^{60}Co γ rays. Corresponding simulations for 220 kVp X rays lead to slightly higher fractions of terminal deletions, but the same parameter values of R and M produce good agreement with the experimental results. For a simulation for 3 Gy irradiation, smaller values of the critical genomic distance M (60 kbp in P1 and 100 kbp in P2) lead to a better consistency with the results of Yamada *et al.*; however, with these parameters, the fractions measured by Nelson *et al.* are quite far away from the calculated distribution, and the overall agreement between simulation and experiment is not improved.

The selection of probability of deletion formation functions has resulted in a constant deletion formation probability from DNA fragments up to about 100 kbp, or corresponding to one chromatin fiber loop. The transition from a constant to a decreasing probability of deletion formation may occur at a somewhat larger or smaller genomic distance; for pairs of breakpoints within the *HPRT* gene, the assumption of a constant misrejoining probability is in accord with measured data. This result may indicate that different mechanisms are in effect for the production of small and large deletions. A possible interpretation is that the *HPRT* gene is located on a chromatin fiber loop of about 0.1 Mbp between nuclear matrix attachment sites; if two breakpoints occur on that loop, the resulting fragment has no attachment point and thus has a rather high and size-independent probability of forming a deletion. For large genomic distances between breakpoints, the attachment to the nuclear matrix maintains the overall integrity of the resulting fragment for a much longer time, resulting in an increased rejoining probability.

The agreement between measured and simulated fractions of small, medium and large deletions for P1 and P2 supports the evaluation of the probability of deletion formation functions and the determination of the parameters R and M on the basis of deletion types. Here the results for the distance-dependent probability functions exhibit smaller discrepancies from the measured data than the deletion type distributions. The striking discrepancy in the fraction of large deletions between experimental results (about 30%) and the calculation using the exponential dependence in function P3 (about 4%) has been found before by Hutchinson (7).

Dose-Dependent Yields of Mutants

The simulated dose-dependent yields of mutants with exon deletions are not intended to be the principal results of the present investigation. The experimental data may be influenced by differences in the survival probabilities of mutants with different deletion types and of normal cells. Such an influence must be expected, particularly with the low surviving fraction of only 6% observed after 2 Gy X irradiation of the radiosensitive human B lymphoblastoid cell line TK6, which was analyzed by Nelson *et al.* (2, 6); at the same dose, about 65% of the cells survived in the experiments of Yamada *et al.* (4). The almost linear dose dependence with a slope of $1.1 \times 10^{-5} \text{ Gy}^{-1}$ for all mutants with exon deletions in the data set of Yamada *et al.* is in better agreement with simulation P2 than with simulation P1. However, both simulations fail to reproduce the rather different distributions of deletion types for the three dose classes in the experiment. This may be a consequence of the small numbers of mutants in the individual categories of doses and deletion types. The dose-dependent changes in the spectrum of *HPRT* mutations induced by ^{137}Cs γ rays in CHO cells were examined recently, yielding a quadratic increase with dose for total deletions and a linear dose response for terminal and intragenic deletions (31).

Probability of Deletion Formation

The maximum probabilities of deletion formation of 0.6 and 0.77 for simulations P1 and P2, respectively, derived for the experimental results of Yamada *et al.* (4) are considerably higher than the factor of 0.125 used by Wu *et al.* in their simulation (8). Their factor was derived from the assumption that 25% of the DSBs participate in misrejoining resulting in either inversions or deletions with the same probability. Recently, fractions of one-half of the initial breaks were found to be misrejoined after X and α -particle irradiation with doses of 80 Gy or more (32). The authors concluded that a misrejoining probability of 50% is valid if sufficient numbers of DSB ends are nearby. Taking into account the fact that clusters of DSBs within about 100 kbp, i.e. within one chromatin fiber loop in our simulation, are not resolved by this method, it can be expected that the misrejoining probability is even higher for such pairs of breaks. Thus the derived maximum values for probability of deletion formation of 0.6 or 0.77 are not in conflict with experimental results. A more detailed analysis of these misrejoining studies is beyond the scope of this work; the present biophysical model is not designed to simulate misrejoining of DSBs in its reported time and dose dependence (33).

The overall agreement in Fig. 6 between the probability of deletion formation for simulation P1 and that of Wu *et al.* (8) for an interaction distance of 0.75 μm in the range between 0.3 and 1.5 Mbp deletion size may seem surprising in view of the rather different results obtained with our simulation model using their parameters. However, this

conformity is attributable to the similar denominators (i.e. distributions of potential deletions and the broken stick fragment), similar numerators (i.e. simulated exon deletion size distributions in accord with experimental data), and the same size dependence ($\sim m^{-3/2}$) in that range. The large variations in the probability of deletion formation of simulation P2 make it evident that the frequency of rather short geometric distances and not the average relationship of genomic and geometric distances determines the result of the simulation, especially for this r^{-3} dependence of the probability of deletion formation. The value of R is influenced by the distribution of geometric distances for a given genomic length which results from the genome model and the minimum distance between parts of the DNA.

Size Distribution of Mutants with Exon Deletions

The simulated cumulative numbers of mutants are found for the most part within the corresponding interval for the measurements of Nelson *et al.* (6) and Yamada *et al.* (4). The largest deviation occurs for the data of Nelson *et al.* and the corresponding simulation P2 between 0.5 and 1.2 Mbp, where the calculated numbers are too small. The calculations, particularly those for simulation P1, show a saturation curve, corresponding to a number of mutants per size interval which decreases with increasing size. The experimental data of Yamada *et al.* have the same behavior, whereas the measurements of Nelson *et al.* exhibit a roughly linear increase with deletion size, corresponding to an almost constant number of mutants per size interval.

Patterns of Deleted Exons

The agreement between the experiments and simulations in the number of total deletions is a consequence of the adaptation of the probability of deletion formation function to the fractions of mutant types. The agreement between the patterns of deleted exons measured by Nelson *et al.* (2) and the corresponding simulations, however, may suggest that the size of the exons and introns determines the pattern of partial deletions of exons. The production of small DNA fragments from pairs of DSBs and subsequent misrejoining with a constant probability is a sufficient explanation for the induction of *HPRT* mutants with exon deletions. This does not exclude other mechanisms from contributing to deletion induction, e.g. loss of an exon after nonhomologous end joining after a single DSB. Further experimental data are needed to allow us to distinguish between the mechanisms involved; measurements with ultrasoft X rays would be particularly beneficial. The discrepancy between the measurements of Yamada *et al.* (4) and the simulations is primarily the high number of measured 5'-terminal deletions; in half of these, a marker site located not more than 1 kbp from the end of the *HPRT* gene is not deleted. This concentration of breakpoints at the 5' end of the gene in the experimental data of Yamada *et al.* still needs to be explained; nuclear matrix attachment sites may be involved.

Patterns of Deleted STS Markers

Differences between experiments and simulations are larger for the patterns of deleted STS markers than for the patterns of deleted exons. Within the present simulation model, these discrepancies between simulation and experiment are not expected to vanish for a different representation of the genome, different assumptions for DSB induction, or different probability of deletion formation functions. The genomic distances between STS markers do not explain the measured patterns of their presence or loss. The marker deletion patterns may reflect a specific spatial organization of the genome in the region of the *HPRT* gene, the influence of nuclear matrix attachment sites surrounding the gene, deviations from the assumed probability of deletion formation, inhomogeneities in the induction of breaks, and additional mechanisms for induction of deletions that were not considered in the simulation. The discordance between the cell lines analyzed in the two experimental data sets may be seen as an indication of a difference in the organization of the genome in that region. The common presence of all STS markers among the mutants with partial deletions may be interpreted to mean that the genome has an increased probability of breakage at certain loci near both ends of the *HPRT* gene.

CONCLUSION

In the framework of present simulation model, the induction of exon deletion mutations at the *HPRT* locus by low-LET radiation is attributed to the nonrandom production of misrejoined DNA fragments between pairs of DSBs. The superposition of the exon-intron pattern of the human *HPRT* gene and DNA fragments being misrejoined with a constant probability up to about 0.1 Mbp in length and a reduced probability for greater lengths leads to distributions of the size, deletion type, and deletion pattern of *HPRT* mutants with exon deletions which are in overall agreement with measured data. The agreement between simulation and measurements is an indication of a dominant mechanism of induction of deletions from pairs of DSBs; however, data for other radiation qualities like ultrasoft X rays must be obtained to assess the contributions of other mechanisms. In contrast to the exon-intron structure of the gene, the genomic loci of the STS marker sites around the *HPRT* gene are not sufficient to explain the patterns of their presence in *HPRT* mutants. The model assumption of a random organization of the genome and random distribution of breakpoints along the genome in the region surrounding the gene within the simulation model appears to be inadequate.

ACKNOWLEDGMENT

This work was supported by the European Community under contract no. FIGH-CT1999-00005 "Low Dose Risk Models".

Received: May 24, 2000; accepted: January 10, 2001

REFERENCES

1. K. Sankaranarayanan, Ionizing radiation and genetic risks, III. Nature of spontaneous and radiation-induced mutations in mammalian *in vitro* systems and mechanisms of induction of mutations by radiation. *Mutat. Res.* **258**, 75–97 (1991).
2. S. L. Nelson, C. R. Giver and A. J. Grossovsky, Spectrum of X-ray induced mutations in the human *hprt* gene. *Carcinogenesis* **15**, 495–502 (1994).
3. M. S. Park, T. Hanks, A. Jaberabansari and D. J. Chen, Molecular analysis of gamma-ray-induced mutations at the *hprt* locus in primary human skin fibroblasts by multiplex polymerase chain reaction. *Radiat. Res.* **141**, 11–18 (1995).
4. Y. Yamada, M. S. Park, R. T. Okinaka and D. J. Chen, Molecular analysis and comparison of radiation-induced large deletions of the *hprt* locus in primary human skin fibroblasts. *Radiat. Res.* **145**, 481–490 (1996).
5. P. Schmidt and J. Kiefer, Deletion-pattern analysis of α -particle and X-ray induced mutations at the *HPRT* locus of V79 Chinese hamster cells. *Mutat. Res.* **421**, 149–161 (1998).
6. S. L. Nelson, I. M. Jones, J. C. Fuscoe, K. Burkhart-Schultz and A. J. Grossovsky, Mapping the end points of large deletions affecting the *hprt* locus in human peripheral blood cells and cell lines. *Radiat. Res.* **141**, 2–10 (1995).
7. F. Hutchinson, Analysis of deletions induced in the genome of mammalian cells by ionizing radiation. *J. Mol. Biol.* **254**, 372–380 (1995).
8. H. Wu, R. K. Sachs and T. C. Yang, Radiation-induced total-deletion mutations in the human *hprt* gene: A biophysical model based on random walk interphase chromatin geometry. *Int. J. Radiat. Biol.* **73**, 149–156 (1998).
9. G. van den Engh, R. K. Sachs and B. Trask, Estimating genomic distance from DNA sequence location in cell nuclei by a random walk model. *Science* **257**, 1410–1412 (1992).
10. R. K. Sachs, G. van den Engh, B. Trask, H. Yokota and J. E. Heast, Random walk/giant-loop model for interphase chromosomes. *Proc. Natl. Acad. Sci. USA* **92**, 2710–2714 (1995).
11. M. Löbrich, B. Rydberg and P. K. Cooper, Repair of x-ray induced DNA double strand breaks in specific Not I restriction fragments in human fibroblasts: Joining of correct and incorrect ends. *Proc. Natl. Acad. Sci. USA* **92**, 12050–12054 (1995).
12. B. Rydberg, Clusters of DNA damage induced by ionizing radiation: Formation of short DNA fragments. II. Experimental detection. *Radiat. Res.* **145**, 200–209 (1996).
13. M. Löbrich, P. K. Cooper and B. Rydberg, Non-random distribution of DNA double-strand breaks induced by particle irradiation. *Int. J. Radiat. Biol.* **70**, 493–503 (1996).
14. H. Newman, K. M. Prise, M. Folkard and B. D. Michael, DNA double-strand break distributions in X-ray and α -particle irradiated V79 cells: Evidence for non-random breakage. *Int. J. Radiat. Biol.* **71**, 347–363 (1997).
15. B. Rydberg, W. R. Holley, I. S. Mian and A. Chatterjee, Chromatin conformation in living cells: Support for a zig-zag model of the 30 nm chromatin fiber. *J. Mol. Biol.* **284**, 71–84 (1998).
16. B. Stenerlöw, E. Hoglund and J. Carlsson, Induction and rejoining of large DNA fragments after ion irradiation. *Radiat. Res.* **151**, 642–648 (1999).
17. W. R. Holley and A. Chatterjee, Clusters of DNA damage induced by ionizing radiation: Formation of short DNA fragments. I. Theoretical modeling. *Radiat. Res.* **145**, 188–199 (1996).
18. W. Friedland, P. Jacob, H. G. Paretzke and T. Stork, Monte Carlo simulation of the production of short DNA fragments by low-linear energy transfer radiation using higher-order DNA models. *Radiat. Res.* **150**, 170–182 (1998).
19. W. Friedland, P. Jacob and H. G. Paretzke, Simulation of DNA fragment distributions after irradiation with photons. *Radiat. Environ. Biophys.* **38**, 39–47 (1999).
20. V. Michalik and M. Begusova, Target model of nucleosome particle for track structure calculations and DNA damage modelling. *Int. J. Radiat. Biol.* **66**, 267–277 (1994).

21. M. Dingfelder, D. Hantke, M. Inokuti and H. G. Paretzke, Electron inelastic-scattering cross-sections in liquid water. *Radiat. Phys. Chem.* **53**, 1–18 (1998).
22. J. A. LaVerne and S. M. Pimblott, Electron energy loss distributions in solid, dry DNA. *Radiat. Res.* **141**, 208–215 (1995).
23. J. A. LaVerne and S. M. Pimblott, Scavenger and time dependences of radicals and molecular products in the electron radiolysis of water: examination of experiments and models. *J. Phys. Chem.* **95**, 3196–3206 (1991).
24. J. E. Turner, R. N. Hamm, H. A. Wright, R. H. Ritchie, J. L. Magee, A. Chatterjee and W. E. Bolch, Studies to link the basic radiation physics and chemistry of liquid water. *Radiat. Phys. Chem.* **32**, 503–510 (1988).
25. G. V. Buxton, C. L. Greenstock, W. P. Helman and A. B. Ross, Critical review of rate constants for reactions of hydrated electrons, hydrogen atoms and hydroxyl radicals in aqueous solution. *J. Phys. Chem. Ref. Data* **17**, 513–886 (1988).
26. F. Ballarini, M. Biaggi, M. Merzagora, A. Ottolenghi, M. Dingfelder, W. Friedland, P. Jacob and H. G. Paretzke, Stochastic aspects and uncertainties in the prechemical and chemical stages of electron tracks in liquid water: A quantitative analysis based on Monte Carlo simulations. *Radiat. Environ. Biophys.* **39**, 179–188 (2000).
27. H. Yokota, G. van den Engh, J. E. Hearst, R. K. Sachs and B. J. Trask, Evidence for the organisation of chromatin in megabase pair-sized loops arranged along a random walk path in the human G₀/G₁ interphase nucleus. *J. Cell Biol.* **130**, 1239–1249 (1995).
28. B. Cedervall, R. Wong, N. Albright, J. Dynlacht, P. Lambin and W. C. Dewey, Methods for the quantification of DNA double-strand breaks determined from the distribution of DNA fragment sizes measured by pulsed-field gel electrophoresis. *Radiat. Res.* **143**, 8–16 (1995); Erratum, *Radiat. Res.* **144**, 122 (1995).
29. K. M. Prise, G. Ahnström, M. Belli, J. Carlsson, D. Frankenberg, J. Kiefer, M. Löbrich, B. D. Michael, J. Nygren and B. Stenerlöv, A review of DSB induction data for varying quality radiations. *Int. J. Radiat. Biol.* **74**, 173–184 (1998).
30. K. Rothkamm and M. Löbrich, Misrejoining of DNA double-strand breaks in primary and transformed human and rodent cells: A comparison between the *HPRT* region and other genomic locations. *Mutat. Res.* **433**, 193–205 (1999).
31. J. L. Schwartz, R. Jordan, J. Sun, H. Ma and A. W. Hsie, Dose-dependent changes in the spectrum of mutations induced by ionizing radiation. *Radiat. Res.* **153**, 312–317 (2000).
32. M. Löbrich, M. Kühne, J. Wetzel and K. Rothkamm, Joining of correct and incorrect DNA double-strand break ends in normal human and ataxia telangiectasia fibroblasts. *Genes Chromosomes Cancer* **27**, 59–68 (2000).
33. M. Kühne, K. Rothkamm and M. Löbrich, No dose dependence of DNA double-strand break misrejoining following α -irradiation. *Int. J. Radiat. Biol.* **76**, 891–900 (2000).